Fission yeast Pot1 and RecQ helicase are required for efficient chromosome segregation

Katsunori Takahashi[1], Ryota Imano[1], Tatsuya Kibe[1,2,3], Hiroyuki Seimiya[4], Yukiko Muramatsu[4], Naoki Kawabata[1], Genki Tanaka[1], Yoshitake Matsumoto[1], Taisuke Hiromoto[1], Yuka Koizumi[1], Norihiko Nakazawa[5], Mitsuhiro Yanagida[5], Masashi Yukawa[1], Eiko Tsuchiya[1], and Masaru Ueno[1]*

[1]Department of Molecular Biotechnology, Graduate School of Advanced Sciences of Matter, Hiroshima University, 1-3-1 Kagamiyama, Higashi-Hiroshima 739-8530, Japan.
[2]Department of Chemistry, Shizuoka University, 836 Oya, Shizuoka, 422-8529, Japan.
[3]Present address: Laboratory for Cell Biology and Genetics, The Rockefeller University, 1230 York Avenue, New York, NY 10065, USA.
[4]Division of Molecular Biotherapy, Cancer Chemotherapy Center, Japanese Foundation for Cancer Research, 3-10-6 Ariake, Koto-Ku, Tokyo 135-8550, Japan.
[5]Graduate School of Biostudies, Kyoto University, Yoshida-Honmachi, Sakyo-Ku, Kyoto 606-8501, Japan.

*Corresponding author: Department of Molecular Biotechnology, Graduate School of Advanced Sciences of Matter, Hiroshima University, 1-3-1 Kagamiyama, Higashi-Hiroshima 739-8530, Japan.
Phone: +81-82-424-7768, Fax: +81-82-424-7000, E-mail: scmueno@hiroshima-u.ac.jp

Running title: *pot1 rqh1* double mutant maintains telomeres

Keywords: Telomere/Pot1/RecQ helicase/Anti-microtubule drug

Abstract

Pot1 is a single-stranded telomere-binding protein that is conserved from fission yeast to mammals. Deletion of *Schizosaccharomyces pombe pot1*$^{+}$ causes immediate telomere loss. *S. pombe* Rqh1 is a homolog of the human RecQ helicase WRN, which plays essential roles in the maintenance of genomic stability. Here, we demonstrate that a *pot1Δ rqh1-hd* (helicase dead) double mutant maintains telomeres that are dependent on Rad51-mediated homologous recombination. Interestingly, the *pot1Δ rqh1-hd* double mutant displays a 'cut' (cell untimely torn) phenotype and is sensitive to the anti-microtubule drug thiabendazole. Moreover, the chromosome ends of the double mutant do not enter the pulsed-field electrophoresis gel. These results suggest that the entangled chromosome ends in the *pot1Δ rqh1-hd* double mutant inhibit chromosome segregation, signifying that Pot1 and Rqh1 are required for efficient chromosome segregation. We also found that POT1-knockdown, WRN-deficient human cells are sensitive to the anti-microtubule drug vinblastine, implying that some of the functions of *S. pombe* Pot1 and Rqh1 may be conserved in their respective human counterparts POT1 and WRN.

INTRODUCTION

Telomeric DNA is composed of repetitive double-stranded DNA followed by a single-stranded (ss) overhang at the 3' end of the G-rich strand. POT1 binds to the ss overhang, and it is required for both chromosomal end protection and telomere length regulation (3). Knockdown of human POT1 by RNA interference leads to apoptosis, chromosomal end-to-end fusion, activation of a DNA damage response, or changes in the overhang structure (16, 41, 46). Knockout of murine Pot1a activates a DNA damage response at the telomeres and elicits aberrant homologous recombination (HR) (15, 44). Removal of chicken POT1 also activates DNA damage responses at telomeres (8). Thus, mammalian POT1 protects telomeres from being recognized as DNA damage.

WRN and BLM are members of the RecQ helicase family (9). Defects in the WRN and BLM genes give rise to the cancer predisposition disorders Werner's syndrome (WS) and Bloom's syndrome (BS), respectively (2). WRN binds to telomeres during the S phase and is required to prevent telomere loss during DNA replication (11). Loss of murine WRN in telomerase-knockout cells promotes recombination within telomeric DNA, escape from cellular senescence, and emergence of immortalized clones; the telomeres of the resultant tumors are maintained via the alternative lengthening of telomeres (ALT) pathway (20). POT1 binds to and stimulates WRN to unwind long telomeric forked duplexes and D-loops *in vitro* (33). In the absence of WRN, human POT1 is required for efficient telomere C-rich strand replication *in vivo* (1). These data suggest a functional relationship between POT1 and WRN in the maintenance of telomeres.

The fission yeast *Schizosaccharomyces pombe* Pot1 was originally identified as a distant homolog of the telomere-binding protein alpha subunit of *Oxytricha nova* (4, 14).

Deletion of *S. pombe pot1*$^{+}$ results in the rapid loss of telomeric DNA and chromosome circularization, making it difficult to study the function of *S. pombe* Pot1 in the maintenance of telomeres (4). In *S. pombe*, deletion of *taz1*$^{+}$, which encodes a telomeric DNA-binding protein, causes massive telomere elongation (10). In contrast, a mutation in *S. pombe rad11*$^{+}$, which encodes the large subunit of RPA, causes telomere shortening (32). Interestingly, a *taz1 rad11* double mutant rapidly loses its telomeric DNA (19). Telomere loss in the *taz1 rad11* double mutant is suppressed by the overexpression of Pot1, implying that the mechanism of telomere loss in the *taz1 rad11* double mutant is related to that in the *pot1* disruptant (19). Telomere loss in the *taz1 rad11* double mutant is also suppressed by the deletion of *rqh1*$^{+}$, a RecQ helicase in *S. pombe* (19). Rqh1 promotes telomere breakage and entanglement in the *taz1* disruptant (34). However, the exact roles of Rqh1 in the maintenance of telomeres are not fully understood. Previous studies of helicase-dead Rqh1 have demonstrated the importance of the helicase activity, but a helicase independent function has been reported as well (17, 29, 35).

In this paper, we analyzed whether the deletion of *rqh1*$^{+}$ suppresses the telomere loss observed in the *pot1* disruptant. We found that the *pot1Δ rqh1-hd* (helicase dead) double mutant maintains telomeres by Rad51-dependent HR. Interestingly, the *pot1Δ rqh1-hd* double mutant was highly sensitive to the anti-microtubule drug thiabendazole (TBZ). Analysis of the phenotypes of the *pot1Δ rqh1-hd* double mutant revealed that Pot1 and Rqh1 are required for efficient chromosome segregation.

RESULTS

pot1Δ rqh1-hd (helicase dead) double mutant is viable, but is sensitive to the anti-microtubule drug thiabendazole (TBZ)

To determine whether the deletion of *rqh1*$^+$ suppresses the telomere loss observed in the *pot1* disruptant, we created 2 types of *pot1 rqh1* double mutant—a *pot1* null *rqh1* null double mutant (*pot1Δ rqh1Δ*) and a *pot1* null *rqh1-K547A* double mutant (*pot1Δ rqh1-hd*). The Rqh1-K547A protein has no helicase activity *in vitro* (21). First, we created these double mutants that contained the plasmid expressing Pot1 because it was difficult to create these double mutants by tetrad analysis and conventional transformation methods. The cells that lost the plasmid were selected on plates containing 5-fluorodeoxyuridine (FUDR) (42). As previously reported, the *pot1Δ rqh1Δ* double mutant was not obtained at 30°C, a standard temperature for *S. pombe* cultivation, showing that the double mutant is synthetically lethal (42). In contrast, we were able to obtain the *pot1Δ rqh1-hd* double mutant at both 25°C and 30°C (Fig. 1A and data not shown). Our results demonstrate that unlike the *pot1Δ rqh1Δ* double mutant, the *pot1Δ rqh1-hd* double mutant is viable. This suggests that the function of Rqh1, other than its helicase activity, is required for the viability of the *pot1* disruptant.

As the *pot1Δ rqh1-hd* cells were viable, we first tested their growth at different temperatures. Although the *pot1Δ rqh1-hd* double mutant grew more slowly than wild-type and *rqh1-hd* cells, it grew at a rate similar to that of *pot1Δ* cells (Fig. 1B), which have circular chromosomes at 25°C. However, the double mutant could not grow at 37°C, indicating that it is sensitive to high temperature (Fig. 1B). Interestingly, we found that the *pot1Δ rqh1-hd* double mutants were highly sensitive to the anti-microtubule drug thiabendazole (TBZ) at 30°C (Fig. 1C), while neither *pot1Δ* nor *rqh1-hd* single mutants showed sensitivity to TBZ at

least at this concentration. Mutants possessing defects in chromosome segregation are sensitive to TBZ, implying that the *pot1Δ rqh1-hd* double mutation affects chromosome segregation (13, 37, 38, 45); therefore, we characterized the TBZ-sensitivity mechanism of the *pot1Δ rqh1-hd* double mutant.

pot1Δ rqh1-hd double mutant can maintain telomeres that are dependent on HR activity

We first assessed whether the *pot1Δ rqh1-hd* double mutant maintains telomeric DNA using a Southern hybridization assay. Interestingly, *pot1Δ rqh1-hd* double mutant showed hybridization signals when the genomic DNA was digested by *EcoR*I and the telomeric probe or the probe containing telomere-associated sequence (TAS1) was used (Fig. 2A and B). This is a sharp contrast to the *pot1Δ* cells that lose both telomeric and TAS1 sequence completely (4). Unlike a typical telomere smear in wild-type strain, the 1.2-kbp telomere band detected in the double mutant was very weak and sharp, implying that only a few telomeric repeats remain. This 1.2-kbp band disappeared by BAL31 nuclease digestion, suggesting that the double mutant has telomeric sequence at the chromosome ends (Fig. 2C). The size of this 1.2-kbp band was longer than expected from simple shortening of the telomere repeat tract. A rearrangement within the terminal subtelomeric fragment could account for this, but further study will be required to understand the exact structure of the telomere ends in the double mutant. Unlike wild-type cells that have telomeric smear, the *pot1Δ rqh1-hd* double mutant had distinct and pronounced signals when TAS1 probe was used, suggesting the amplification of the TAS1 containing subtelomere sequence (Fig. 2B and C). To test this possibility, we carried out Southern hybridization assay with *Nsi*I-digested genomic DNA. The sizes of the TAS1 containing-terminal fragments of the wild-type cells are around 2 to 6-kbp. In contrast,

the size of the TAS1 containing-terminal fragment of the *pot1Δ rqh1-hd* double mutant was about 23-kbp, suggesting that the size of the terminal fragments is longer than 23-kbp (data not shown). Based on the size of the *EcoR*I digested TAS1 containing fragment (about 1.6-kbp), we assume that the *Nsi*I digested terminal fragments have TAS1 containing repeats at least more than 10 (Fig. 2D model). This chromosome-end structure may be similar to the *S. cerevisiae* type I survivors lacking telomerase, in which the subtelomeric sequences are amplified at telomere ends (22). The band pattern of the three independent *pot1Δ rqh1-hd* double mutants did not significantly change during 3 re-streaks, showing that the chromosome ends of the double mutants are not vigorously rearranged at 25°C (data not shown).

Telomere-telomere recombination is elevated in WRN-deficient (homolog of Rqh1), telomerase-knockout mouse cells (20); moreover, murine Pot1a-deficient cells exhibit aberrant HR at telomeres (44). These facts imply that telomere-telomere recombination is elevated in the *pot1Δ rqh1-hd* double mutant. In *S. pombe*, Rad51, originally named as Rhp51, plays important roles in HR (28). To test the contribution of HR in the maintenance of telomeres in the double mutant, we created a *pot1Δ rqh1-hd rad51Δ* triple mutant. The *pot1Δ rqh1-hd rad51Δ* triple mutant completely lost the hybridization signal when the DNA probe contained telomeric and TAS1 sequence, showing that the chromosome ends of the double mutants are maintained by HR (Fig. 2E).

Chromosome ends of the *pot1Δ rqh1-hd* double mutant are entangled

Since the chromosomes of the *pot1Δ* cells are circularized, the chromosomes of the *pot1Δ rqh1-hd* double mutants were analyzed using pulsed-field gel electrophoresis (PFGE)

(Fig. 3A and B). The *Not*I-digested fragments M, L, I, and C, which are located at the ends of chromosomes I and II, were detected in the *rqh1-hd* single mutant. In contrast, the *pot1Δ rqh1-hd* double mutant had almost no M, L, I, or C signals. The centromere proximal fragment next to the C fragment was detected when the Nbs1 probe was used as an internal control (Fig. 3A and B). Moreover, the ethidium bromide-staining pattern showed that the bulk DNA entered the gel, suggesting that only the chromosome-end fragments were unable to enter the gel. DNA with branched structures, such as replicating DNA forks or recombination intermediates, cannot enter a pulsed-field gel. Our results suggest that the chromosome ends of the double mutant have branched structures, but the internal chromosome fragments do not contain these DNA structures. Similar to the *pot1Δ rqh1-hd* double mutant, the chromosomes of the *taz1* disruptant do not enter the pulsed-field gel at 20°C, suggesting that the telomeres in the *taz1* disruptant are entangled at this temperature (23); however, unlike the *pot1Δ rqh1-hd* double mutant, the *taz1* disruptant is not sensitive to TBZ (23), suggesting that the type of entanglement in the *pot1Δ rqh1-hd* double mutant is different from that in the *taz1* disruptant at 20°C. PFGE of the *pot1Δ rqh1-hd rad51Δ* triple mutant showed that the chromosomes of this mutant were circularized (Fig. 3C).

pot1Δ rqh1-hd double mutant has RPA foci

Our results suggest that the stalled replication forks and/or recombination intermediates may exist at the chromosome ends in the *pot1Δ rqh1-hd* double mutant. As RPA binds to the ssDNA generated during DNA replication, recombination, and damage, we monitored the localization of RPA in the double mutant by using Rad11 that was endogenously tagged with GFP (39). Most of the wild-type cells and approximately 70% of

the *rqh1-hd* single mutants had no RPA foci (Fig. 4A and B). In contrast, approximately 80% of the *pot1Δ rqh1-hd* double mutants had RPA foci, suggesting that ssDNA accumulates in the double mutant. The accumulation of ssDNA may activate DNA damage checkpoint. Many of the *pot1Δ rqh1-hd* double mutant cells are elongated and the elongation of the double-mutant cells is suppressed by deletion of $chk1^{+}$, suggesting that DNA-damage checkpoint is activated in the double mutant (Fig. 4A and data not shown). We also found that approximately 70% of the *pot1* single mutants had no RPA foci, suggesting that circular chromosomes do not induce an excess amount of ssDNA (data not shown). Next, we tested the colocalization between RPA and the telomeres by using cells expressing endogenously tagged Taz1-YFP (a telomeric marker) and Ssb2-CFP (the middle subunit of RPA) (39). The majority of the Taz1 foci in the asynchronous double-mutant cells either colocalized with or localized adjacent to the Ssb2 foci, while most of the Taz1 foci in the *pot1Δ rqh1-hd* double mutant expressing Pot1 from a plasmid did not colocalize with the Ssb2 foci (Fig. 4C and D). This suggests that the RPA foci are produced at and/or near telomeres in the double mutant, and these foci may represent recombination intermediates, stalled replication forks, and/or ss telomeric overhangs (39). Interestingly, the Taz1 foci were adjacent to the RPA foci on the chromosomal bridge in the *pot1Δ rqh1-hd* double mutant (Fig. 4C right panel), suggesting that the RPA foci produced near the telomeres exist during the M phase. We also tested the colocalization between RPA and Rad22 by using cells expressing endogenously tagged Rad22-YFP and Ssb2-CFP (the middle subunit of RPA) (26). Fission yeast Rad22, a Rad52 homolog, is a DNA repair protein required for HR and binds to the *taz1Δ* (unprotected) telomeres (7, 40). The most of the Rad22 foci in the asynchronous double-mutant cells colocalized with the Ssb2 foci, suggesting that the RPA foci produced at and/or near

telomeres in the double mutant represent recombination intermediates (Fig. 4E and F).

pot1Δ rqh1-hd double mutant has RPA foci during the M phase

We monitored the RPA foci in the double mutant during the M phase because our results suggested that entangled telomeres caused the M phase defect. While the *rqh1-hd* single mutant did not have RPA foci during the M phase, the RPA foci appeared on chromosomal bridges during anaphase in the *pot1Δ rqh1-hd* double mutant at a high frequency (Fig. 5A and B), suggesting that ssDNA exists during anaphase in the double mutant. Similar to the case of the RPA foci, the Rad22 foci appeared on chromosomal bridges during anaphase in the *pot1Δ rqh1-hd* double mutant at a high frequency, but not in the *rqh1-hd* single mutant (data not shown), suggesting that the recombination intermediates exist during anaphase in the double mutant. We found that *pot1Δ rqh1-hd rad51Δ* triple mutant, which has circular chromosomes, has almost no RPA foci on the chromosome bridge during anaphase (Fig. 5B), suggesting that the foci detected in the *pot1Δ rqh1-hd* double mutant are produced at the chromosome ends. Importantly, the RPA foci detected in the *pot1Δ rqh1-hd* double mutant existed before the cells entered anaphase, showing that the RPA foci are not produced during anaphase. This ruled out the possibility that the RPA foci are produced by a breakage-fusion-bridge cycle. Our results suggest that the DNA damage checkpoint activated in the *pot1Δ rqh1-hd* double mutant resulting in cell cycle arrest at the G2/M boundary. However, a subset of cells eventually break through the arrest to enter mitosis.

The *rqh1* mutant does not fully activate known checkpoints and shows a ‘cut’ (cell untimely torn) phenotype where chromosomes are bisected by the septum when the cells are released from HU arrest (35). Holliday junctions (HJ) or other recombination intermediates

that exist during the M phase are thought to be the cause of the cut phenotype (12). We were able to detect RPA foci during the M phase in the *rqh1-hd* single mutant after releasing the cells from HU arrest (Fig. 5C and D), suggesting that the RPA foci detected during the M phase represent recombination intermediates. These foci are similar to those detected in the *pot1Δ rqh1-hd* double mutant (Fig. 5A and B), implying that the accumulation of ssDNA in the *pot1Δ rqh1-hd* double mutant during the M phase represents recombination intermediates.

As the *rqh1* single mutant has a defect in nucleolar segregation (43), RPA foci in the *pot1Δ rqh1-hd* double mutant during the M phase may also be produced at rDNA. To test this possibility, we analyzed the colocalization between rDNA and RPA during the M phase by using cells expressing endogenously tagged Gar2-GFP, a marker of rDNA, and Rad11-mRFP (29). We observed 18 cells of the *pot1Δ rqh1-hd* double mutant during the M phase. We detected only one example of the side by side localization between Rad11-mRFP and Gar2-GFP during the M phase, but we could not detect colocalization between Rad11-mRFP and Gar2-GFP during the M phase (Fig. 5E), indicating that the RPA foci detected in the *pot1Δ rqh1-hd* double mutant during the M phase are not produced inside of the rDNA.

pot1Δ rqh1-hd double mutant has a chromosome segregation defect

The ssDNA observed during the M phase in the double mutant, possibly recombination intermediates, may cause a chromosome segregation defect because these structure will physically link sister chromatids together. Indeed, the frequency of the cut phenotype of the *pot1Δ rqh1-hd* double mutant was significantly higher than in the *rqh1-hd* single mutant in the absence of TBZ (Fig. 6A). We also studied the chromosome segregation defect in the presence of TBZ because the *pot1Δ rqh1-hd* double mutant is sensitive to TBZ.

In the presence of a low concentration of TBZ (17.5 μg/mL), the frequency of the cut phenotype in the double mutant was significantly higher than of the *rqh1-hd* single mutant (Fig. 6A and B). At a high concentration of TBZ (50 μg/mL), the frequency of chromosome non-disjunction increased in the double mutant, but not in the *rqh1-hd* single mutant. These results suggest that the fully or partially functional mitotic spindle can segregate chromosomes even though the chromosome ends are entangled, causing the cut phenotype. At a high concentration of TBZ (50 μg/mL), the destabilized mitotic spindle cannot segregate the entangled chromosomes, resulting in chromosome non-disjunction (Fig. 6C). On the basis of these data, we conclude that entanglement of the chromosome ends in the double mutant is the cause of its sensitivity to TBZ. *trt1* single mutant was not sensitive to TBZ when cells were grown at liquid culture both at early generations that have telomeric DNA and at late generations that have linear chromosomes by recombination dependent manner, demonstrating that the telomere recombination itself is not the cause of the TBZ sensitivity (Ueno, M., unpublished observations). However, it has been reported the third type of *trt1* survivor called HAATI (18). This survivor shares some phenotypes with the *pot1Δ rqh1-hd* double mutant, including HR-dependent maintenance of the chromosome ends and stacking chromosomes at wells of the pulsed-field gel. Therefore, this survivor may have similar chromosome segregation defects to the *pot1Δ rqh1-hd* double mutant.

Simultaneous inactivation of human POT1 and WRN enhances cellular sensitivity to the anti-microtubule drug vinblastine

Many of the telomere-binding proteins in *S. pombe* are conserved in humans (26). This prompted us to assess whether human Pot1 and WRN (homolog of Rqh1) are required

for viability in the presence of the anti-microtubule drug vinblastine that inhibits microtubule polymerization. In order to address this issue, we first reconstituted wild-type WRN in SV40-transformed, WRN-deficient W-V cells (Fig. 7A). The resulting infectant (W-V/WRN) and the control cell line (W-V/pLPC) were further transfected with siRNAs to deplete the POT1 protein (Fig. 7B). Under these conditions, cellular sensitivity to vinblastine was monitored. As shown in Figure 7C (lower panel), POT1 knockdown enhanced the cytotoxicity of vinblastine to some extent in the W-V/WRN cells. These data indicate that, in human cells, depletion of POT1 alone can enhance the deleterious effect of vinblastine. Importantly, this effect of POT1 depletion on the sensitivity to the drug was more evident under WRN-deficient conditions (Fig. 7C, upper panel). In fact, sensitization to vinblastine, which was defined as a ratio of 50% growth inhibitory concentrations (IC50) of control siRNA-treated cells to those of POT1 knockdown cells, was higher in W-V/pLPC cells than that in W-V/WRN cells (Fig. 7D). These observations indicate that deficiencies in POT1 and WRN increase the sensitivity of cultured human cells to the anti-microtubule drug vinblastine.

DISCUSSION

Telomeres are maintained by HR in the *pot1Δ rqh1-hd* double mutant

The *S. pombe pot1* disruptant suffers an immediate loss of telomeric DNA followed by fusion of its chromosome ends (4). In this study, we found that the *pot1Δ rqh1-hd* double mutant could maintain its telomeres. As the Pot1 complex is required for the recruitment of telomerase to the telomere (26, 39), it is likely that telomerase cannot function in the *pot1Δ rqh1-hd* double mutant. Indeed, telomeres in the *pot1Δ rqh1-hd* double mutant were maintained by HR. Rqh1 inhibits inappropriate recombination (35); therefore, the hyper-recombination phenotype of the *rqh1-hd* mutant is likely to increase the probability of HR at the chromosome ends when $pot1^+$ is deleted. This could be the reason why the double mutant can maintain its telomeres. The *S. cerevisiae* RecQ helicase Sgs1 is involved in the degradation of the 5' strand at both double strand breaks (DSB) and at telomeres (6, 25, 47). These facts imply that Rqh1 may be involved in the degradation of telomeres in *pot1Δ* cells. Unlike *pot1Δ rqh1-hd* double mutants, the *pot1Δ rqh1* double mutant is synthetically lethal (42), suggesting that the helicase-independent function of Rqh1 is important for viability in the absence of Pot1. As Rqh1 binds to several proteins, such as Top3 and RPA (19, 21), helicase-dead Rqh1 may have a function with these or other proteins to maintain the viability of the *pot1Δ* cells. Further investigation is required to understand the reason for the synthetic lethality.

pot1Δ rqh1-hd double mutant is sensitive to TBZ and has defects in chromosome segregation

The progression of anaphase is delayed in cells lacking Rqh1 and the cells have

lagging chromosomal DNA, which is apparent at the rDNA loci (43). However, the *rqh1* mutant is not sensitive to TBZ at the concentration we tested, suggesting that the segregation defect of the rDNA loci in the *rqh1* mutant is not catastrophic to the cells. Interestingly, the *pot1Δ rqh1-hd* double mutant was highly sensitive to TBZ. PFGE analysis of the *Not*I-digested genomic DNA suggests that the chromosome ends of the double mutant are entangled. The *pot1Δ rqh1-hd* double mutant displayed RPA foci, a marker of DNA recombination, damage, or stalled replication forks, at a high frequency in asynchronous cells (mainly the G2 phase) and in M phase cells, and many Taz1 foci and Rad22 foci colocalized with the RPA foci, suggesting that the recombination intermediates are produced at and/or near the telomeres. The RPA foci did not colocalize with the rDNA marker Gar2, suggesting that the defects in the *pot1Δ rqh1-hd* double mutant are not due to problems with rDNA. The recombination intermediates that were produced following the release from HU arrest in the *rqh1* mutant inhibit proper chromosome segregation, resulting in the cut phenotype. We detected RPA foci during the M phase in the *rqh1-hd* single mutant after the cells were released from HU arrest, suggesting that these RPA foci represent recombination intermediates. The *pot1Δ rqh1-hd* double mutant also displayed the cut phenotype; moreover, RPA foci were detected during the M phase in the double mutant. These facts imply that DNA entanglement produced at the chromosome ends in the *pot1Δ rqh1-hd* double mutant may have a similar structure to those produced in the *rqh1-hd* single mutant following release from HU arrest, which is suggested to be a HJ. However, as human Pot1 and WRN are required for efficient DNA replication (1, 11), we do not rule out the possibility that RPA foci in the *pot1Δ rqh1-hd* double mutant represent stalled replication forks at and/or near the telomeres. But the stalled replication forks would cause DNA breaks, which would become

the substrates for HR.

As the *pot1Δ rqh1-hd rad51Δ* triple mutant has circular chromosomes, it is expected that the triple mutant is not sensitive to TBZ because its chromosomes are not entangled. However, the *rad51* single mutant is sensitive to TBZ (30), making it difficult to compare the phenotypes of the *pot1Δ rqh1-hd* double mutant and the *pot1Δ rqh1-hd rad51Δ* triple mutant. Indeed, the *pot1Δ rqh1-hd rad51Δ* triple mutant was sensitive to TBZ, but the TBZ sensitivity of the triple mutant was slightly weaker than the double mutant, suggesting that the entangled chromosomal ends in the double mutant affected the TBZ sensitivity (data not shown). The *ccq1* single mutant shares some phenotypes with the *pot1Δ rqh1-hd* double mutant, including HR-dependent telomere maintenance, RPA foci, and the cut phenotype (39). However, unlike the *pot1Δ rqh1-hd* double mutant, the chromosome-end fragments of the *ccq1* single mutant and *ccq1 rqh1* double mutant can enter the pulsed-field gel, suggesting that the chromosome ends of the *ccq1* single mutant and *ccq1 rqh1* double mutant are not severely entangled.

Clinical implications of hypersensitivity to anti-microtubule drugs

We found that the knockdown of POT1 in SV40-immortalized WRN deficient cells rendered the cells more sensitive to vinblastine. These observations are similar to those of the *S. pombe pot1Δ rqh1-hd* double mutant, implying that the functions of *S. pombe* Pot1 and Rqh1 may be conserved in their respective human counterparts, POT1 and WRN. However, our telomere fluorescence *in situ* hybridization analysis on metaphase spreads revealed that POT1 depletion in W-V cells did not induce end-to-end fusions or entanglement-like features of chromosomes (Seimiya, H., unpublished observations). These observations suggest that

either POT1 depletion in WRN deficient cells is not enough to induce the same phenotype as observed in *S. pombe* or that the underlying mechanisms for the higher sensitivities to TBZ in *S. pombe* and vinblastine in humans may not completely overlap with each other. Nevertheless, our finding that depletion of POT1 alone in human cells can enhance their sensitivity to vinblastine suggests that human POT1 is involved in chromosome segregation.

Since anti-microtubule compounds are commonly used as anticancer drugs in the clinical setting, our results suggest a novel approach for sensitizing cancer cells to anti-microtubule drugs by inactivating either POT1 or both POT1 and WRN. Indeed, we observed that a human cancer cell line expressing low levels of POT1 and WRN proteins exhibits a relatively higher sensitivity to anti-microtubule drugs (Muramatsu, Y., Yamori, Y., and Seimiya, H., unpublished observations).

MATERIALS AND METHODS

Strain construction and growth media

The strains used in this report are listed in Table I. The *pot1::KanMX rqh1-K547A* double mutant (*pot1Δ rqh1-hd*) was created as follows. First, the *pot1Δ rqh1-hd* double mutant expressing Pot1 from a plasmid containing the *LEU2* gene (nmt1-pot1-V5, gift from Peter Baumann) was created by the transformation of *rqh1-hd* cells (YK002) expressing Pot1 from the plasmid nmt1-pot1-V5 using the *pot1::KanMX* disruption fragment, in which the complete open reading frame (ORF) is replaced by the *KanMX* gene (gift from Peter Baumann). The plasmid nmt1-pot1-V5 in the *pot1Δ rqh1-hd* double mutant was then replaced by the plasmid pPC27-pot1-3HA containing the *HSV-tk* and *ura4*$^{+}$ genes as negative selection markers (a gift from Peter Baumann). The *pot1Δ rqh1-hd* double mutant that lost the plasmid pPC27-pot1-3HA was selected on YEA plates containing 50 μM 5-fluorodeoxyuridine (FUDR) or 2 g/L 5-fluoroorotic acid (5-FOA) at 25°C or 30°C. The *pot1::KanMX rqh1-K547A rad51-d* triple mutant (*pot1Δ rqh1-hd rad51Δ*) was created as follows. The *pot1Δ rqh1-hd rad51Δ* triple mutant containing the Pot1 plasmid pPC27-pot1-3HA was created by transforming the *pot1Δ rqh1-hd* double mutant expressing Pot1 from pPC27-pot1-3HA with the *rad51::LUE2* disruption fragment, in which the *LUE2* cassette is inserted in the *Nhe*I site of the *rad51* gene. The *pot1Δ rqh1-hd rad51Δ* triple mutant that does not have pPC27-pot1-3HA was selected on YEA plates containing 2 g/L 5-FOA. Cells were grown in YEA medium (0.5% yeast extract, 3% glucose, and 40 μg/mL adenine) at the indicated temperature.

Measurement of telomere length

Telomere length was measured using Southern hybridization according to a previously described procedure (10) with an AlkPhos Direct Kit module (GE Healthcare). A 450-bp synthetic telomere fragment (24), and a TAS1 or a TAS1 plus telomere fragments derived from pNSU70 (36) were used as probes. A 450-bp telomeric DNA probe was labeled with [α-^{32}P]dCTP (Parkin Elmer) by using Rediprime II DNA Labelling System (GE Healthcare). The membrane was hybridized overnight with hybridization buffer (GE Healthcare Rapid-Hyb Buffer) and the 10 ng probe at 37°C.

Pulsed-field gel electrophoresis

PFGE was performed as described by Baumann et al. (5). For the detection of *Not*I-digested chromosomes, *Not*I-digested *S. pombe* chromosomal DNA was fractionated in a 1% agarose gel with a 0.5× TBE (50 mM Tris-HCl, 5 mM boric acid, and 1 mM EDTA, pH 8.0) buffer at 14°C using the CHEF Mapper PFGE system at 6 V/cm (200 V) and a pulse time of 60–120 s for 24 h. DNA was visualized by staining with ethidium bromide (1 μg/mL) for 30 min.

Microscopy

Microscope images of living cells were obtained using an AxioCam digital camera (Zeiss) connected to an Axiovert 200M microscope (Zeiss) with a Plan-Apo-chromat 63X NA 1.4 objective lens. Pictures were captured and analyzed using AxioVision Rel. 4.3 Software (Zeiss). A glass-bottom dish (Iwaki) coated with 5 mg/mL lectin from *Bandeiraea simplicifolia* BS-I (Sigma) or 10 mg/mL concanavalin A (Wako). The time-lapse images of tagged proteins in living cells were taken at 30 s intervals at 30°C.

siRNA knockdown and drug sensitivity assay

The SV40-immortalized WRN-deficient human cells (W-V cells, kindly provided by Kiyoji Tanaka) were grown in Dulbecco's modified Eagle's medium supplemented with 10% heat-inactivated fetal bovine serum and 100 μg/mL kanamycin in a humidified atmosphere of 5% CO_2 at 37°C. Retroviral infection was performed as previously described (Seimiya et al., MCB, 2004) using the pLPC/FLAG-WRN retroviral vector (kindly provided by Jan Karlseder) (Crabbe et al., Science, 2004). Following infection, the cells were selected using 2 μg/mL puromycin (Sigma). To maintain the established cell lines, 0.5 μg/mL puromycin was added to the growth medium. The Stealth siRNAs to POT1 (#1: 5′-AAAGUAGACAUUCAUUUGAAAGCGG-3′ and #3: 5′-UAAGAAAGCUUCCAACCUUCAGAGA-3′) were purchased from Invitrogen. As a control, Stealth RNAi Negative Control LO GC (12935-200) was used. These siRNAs were transiently introduced into the cells using Lipofectamine RNAiMAX (Invitrogen) according to the manufacturer's instructions. Knockdown efficiency was determined using Western blot analysis as described below. Cellular sensitivity to vinblastine (48-h exposure) was determined by measuring the relative cell number at the end of the drug treatment with the CellTiter 96 AQueous One Solution Cell Proliferation Assay (Promega) according to the manufacturer's instructions.

Western blot analysis

Cells were washed in ice-cold phosphate-buffered saline (PBS) and lysed in TNE buffer (10 mM Tris-HCl, pH 7.8, 1% NP-40, 150 mM NaCl, and 1 mM EDTA) and 1:40 volume of protease inhibitor cocktails (Sigma) on ice for 30 min. After centrifugation at 12,000 × *g* for

10 min at 4°C, the supernatant was collected as the TNE lysate. Nuclear extracts were prepared using a CelLytic NuCLEAR Extraction Kit (Sigma). For the detection of POT1, the TNE lysates were immunoprecipitated using rabbit anti-POT1 antiserum D6442 (27) or normal rabbit immunoglobulin G (Santa Cruz Biotechnology). For the detection of WRN, the lysate was immunoprecipitated using rabbit anti-WRN ab-200 (Abcam) or mouse anti-FLAG (M2, Sigma). The immunocomplexes were subjected to western blot analysis using affinity-purified anti-POT1 D6442 or anti-WRN (ab-200) as a primary antibody and the TrueBlot anti-rabbit IgG horseradish peroxidase (eBioscience) as a secondary antibody, respectively. Signals were detected using the ECL Detection System (GE Healthcare).

ACKNOWLEDGEMENTS

We wish to thank P. Baumann, J. Murray, K. Tomita, M. Ferreira, J. Cooper, J. Karlseder, K. Tanaka, T. Ohno, T. Toda, R. Tesin, T. Sakuno, Y. Watanabe, Shao-Win Wang, and the National Bioresource Project Japan for providing the plasmids and strains. We thank M. Mizunuma and K. Mizuta for their help in microscopy. This work was supported by Grants-in-Aid for Scientific Research on Priority Areas from the Ministry of Education, Science, Sports and Culture of Japan to Masaru Ueno. Tatsuya Kibe is a Research Fellow of the Japan Society for the Promotion of Science.

REFERENCES

1. **Arnoult, N., C. Saintome, I. Ourliac-Garnier, J. F. Riou, and A. Londono-Vallejo.** 2009. Human POT1 is required for efficient telomere C-rich strand replication in the absence of WRN. Genes Dev. **23:**2915-24.
2. **Bachrati, C. Z., and I. D. Hickson.** 2003. RecQ helicases: suppressors of tumorigenesis and premature aging. Biochem. J. **374:**577-606.
3. **Baumann, P.** 2006. Are mouse telomeres going to pot? Cell **126:**33-6.
4. **Baumann, P., and T. R. Cech.** 2001. Pot1, the putative telomere end-binding protein in fission yeast and humans. Science **292:**1171-5.
5. **Baumann, P., and T. R. Cech.** 2000. Protection of telomeres by the Ku protein in fission yeast. Mol. Biol. Cell. **11:**3265-75.
6. **Bonetti, D., M. Martina, M. Clerici, G. Lucchini, and M. P. Longhese.** 2009. Multiple pathways regulate 3' overhang generation at *S. cerevisiae* telomeres. Mol Cell **35:**70-81.
7. **Carneiro, T., L. Khair, C. C. Reis, V. Borges, B. A. Moser, T. M. Nakamura, and M. G. Ferreira.** Telomeres avoid end detection by severing the checkpoint signal transduction pathway. Nature **467:**228-32.
8. **Churikov, D., C. Wei, and C. M. Price.** 2006. Vertebrate POT1 restricts G-overhang length and prevents activation of a telomeric DNA damage checkpoint but is dispensable for overhang protection. Mol. Cell. Biol. **26:**6971-82.
9. **Cobb, J. A., and L. Bjergbaek.** 2006. RecQ helicases: lessons from model organisms. Nucleic Acids Res. **34:**4106-14.

10. **Cooper, J. P., E. R. Nimmo, R. C. Allshire, and T. R. Cech.** 1997. Regulation of telomere length and function by a Myb-domain protein in fission yeast. Nature **385:**744-7.

11. **Crabbe, L., R. E. Verdun, C. I. Haggblom, and J. Karlseder.** 2004. Defective telomere lagging strand synthesis in cells lacking WRN helicase activity. Science **306:**1951-3.

12. **Doe, C. L., J. Dixon, F. Osman, and M. C. Whitby.** 2000. Partial suppression of the fission yeast *rqh1*$^-$ phenotype by expression of a bacterial Holliday junction resolvase. EMBO J. **19:**2751-62.

13. **Ekwall, K., E. R. Nimmo, J. P. Javerzat, B. Borgstrom, R. Egel, G. Cranston, and R. Allshire.** 1996. Mutations in the fission yeast silencing factors *clr4*$^+$ and *rik1*$^+$ disrupt the localisation of the chromo domain protein Swi6p and impair centromere function. J. Cell. Sci. **109 (Pt 11):**2637-48.

14. **Gray, J. T., D. W. Celander, C. M. Price, and T. R. Cech.** 1991. Cloning and expression of genes for the *Oxytricha* telomere-binding protein: specific subunit interactions in the telomeric complex. Cell **67:**807-14.

15. **Hockemeyer, D., J. P. Daniels, H. Takai, and T. de Lange.** 2006. Recent expansion of the telomeric complex in rodents: Two distinct POT1 proteins protect mouse telomeres. Cell **126:**63-77.

16. **Hockemeyer, D., A. J. Sfeir, J. W. Shay, W. E. Wright, and T. de Lange.** 2005. POT1 protects telomeres from a transient DNA damage response and determines how human chromosomes end. EMBO J. **24:**2667-78.

17. **Hope, J. C., S. M. Mense, M. Jalakas, J. Mitsumoto, and G. A. Freyer.** 2006. Rqh1

blocks recombination between sister chromatids during double strand break repair, independent of its helicase activity. Proc. Natl. Acad. Sci. U. S. A. **103:**5875-80.

18. **Jain, D., A. K. Hebden, T. M. Nakamura, K. M. Miller, and J. P. Cooper.** HAATI survivors replace canonical telomeres with blocks of generic heterochromatin. Nature **467:**223-7.

19. **Kibe, T., Y. Ono, K. Sato, and M. Ueno.** 2007. Fission yeast Taz1 and RPA are synergistically required to prevent rapid telomere loss. Mol. Biol. Cell. **18:**2378-87.

20. **Laud, P. R., A. S. Multani, S. M. Bailey, L. Wu, J. Ma, C. Kingsley, M. Lebel, S. Pathak, R. A. DePinho, and S. Chang.** 2005. Elevated telomere-telomere recombination in WRN-deficient, telomere dysfunctional cells promotes escape from senescence and engagement of the ALT pathway. Genes Dev. **19:**2560-70.

21. **Laursen, L. V., E. Ampatzidou, A. H. Andersen, and J. M. Murray.** 2003. Role for the fission yeast RecQ helicase in DNA repair in G2. Mol. Cell. Biol. **23:**3692-705.

22. **Lundblad, V., and E. H. Blackburn.** 1993. An alternative pathway for yeast telomere maintenance rescues *est1*$^-$ senescence. Cell **73:**347-60.

23. **Miller, K. M., and J. P. Cooper.** 2003. The telomere protein Taz1 is required to prevent and repair genomic DNA breaks. Mol. Cell **11:**303-13.

24. **Miller, K. M., O. Rog, and J. P. Cooper.** 2006. Semi-conservative DNA replication through telomeres requires Taz1. Nature **440:**824-8.

25. **Mimitou, E. P., and L. S. Symington.** 2008. Sae2, Exo1 and Sgs1 collaborate in DNA double-strand break processing. Nature **455:**770-4.

26. **Miyoshi, T., J. Kanoh, M. Saito, and F. Ishikawa.** 2008. Fission yeast Pot1-Tpp1 protects telomeres and regulates telomere length. Science **320:**1341-4.

27. **Muramatsu, Y., H. Tahara, T. Ono, T. Tsuruo, and H. Seimiya.** 2008. Telomere elongation by a mutant tankyrase 1 without TRF1 poly(ADP-ribosyl)ation. Exp. Cell. Res. **314:**1115-24.

28. **Muris, D. F., K. Vreeken, A. M. Carr, B. C. Broughton, A. R. Lehmann, P. H. Lohman, and A. Pastink.** 1993. Cloning the *RAD51* homologue of *Schizosaccharomyces pombe*. Nucleic Acids Res. **21:**4586-91.

29. **Murray, J. M., H. D. Lindsay, C. A. Munday, and A. M. Carr.** 1997. Role of *Schizosaccharomyces pombe* RecQ homolog, recombination, and checkpoint genes in UV damage tolerance. Mol. Cell. Biol. **17:**6868-75.

30. **Nakamura, K., A. Okamoto, Y. Katou, C. Yadani, T. Shitanda, C. Kaweeteerawat, T. S. Takahashi, T. Itoh, K. Shirahige, H. Masukata, and T. Nakagawa.** 2008. Rad51 suppresses gross chromosomal rearrangement at centromere in *Schizosaccharomyces pombe*. EMBO J. **27:**3036-46.

31. **Nakamura, T. M., J. P. Cooper, and T. R. Cech.** 1998. Two modes of survival of fission yeast without telomerase. Science **282:**493-6.

32. **Ono, Y., K. Tomita, A. Matsuura, T. Nakagawa, H. Masukata, M. Uritani, T. Ushimaru, and M. Ueno.** 2003. A novel allele of fission yeast *rad11* that causes defects in DNA repair and telomere length regulation. Nucleic Acids Res. **31:**7141-9.

33. **Opresko, P. L., P. A. Mason, E. R. Podell, M. Lei, I. D. Hickson, T. R. Cech, and V. A. Bohr.** 2005. POT1 stimulates RecQ helicases WRN and BLM to unwind telomeric DNA substrates. J. Biol. Chem. **280:**32069-80.

34. **Rog, O., K. M. Miller, M. G. Ferreira, and J. P. Cooper.** 2009. Sumoylation of RecQ helicase controls the fate of dysfunctional telomeres. Mol. Cell **33:**559-69.

35. **Stewart, E., C. R. Chapman, F. Al-Khodairy, A. M. Carr, and T. Enoch.** 1997. *rqh1*$^{+}$, a fission yeast gene related to the Bloom's and Werner's syndrome genes, is required for reversible S phase arrest. EMBO J. **16:**2682-92.

36. **Sugawara, N.** 1988. DNA Sequences at the Telomeres of the Fission Yeast *S. pombe*. Ph. D. Thesis. Cambrige, MA: Harvard University.

37. **Tanaka, K., J. Nishide, K. Okazaki, H. Kato, O. Niwa, T. Nakagawa, H. Matsuda, M. Kawamukai, and Y. Murakami.** 1999. Characterization of a fission yeast SUMO-1 homologue, pmt3p, required for multiple nuclear events, including the control of telomere length and chromosome segregation. Mol. Cell. Biol. **19:**8660-72.

38. **Tatebayashi, K., J. Kato, and H. Ikeda.** 1998. Isolation of a *Schizosaccharomyces pombe rad21ts* mutant that is aberrant in chromosome segregation, microtubule function, DNA repair and sensitive to hydroxyurea: possible involvement of Rad21 in ubiquitin-mediated proteolysis. Genetics **148:**49-57.

39. **Tomita, K., and J. P. Cooper.** 2008. Fission yeast Ccq1 is telomerase recruiter and local checkpoint controller. Genes Dev. **22:**3461-74.

40. **van den Bosch, M., K. Vreeken, J. B. Zonneveld, J. A. Brandsma, M. Lombaerts, J. M. Murray, P. H. Lohman, and A. Pastink.** 2001. Characterization of RAD52 homologs in the fission yeast *Schizosaccharomyces pombe*. Mutat. Res. **461:**311-23.

41. **Veldman, T., K. T. Etheridge, and C. M. Counter.** 2004. Loss of hPot1 function leads to telomere instability and a cut-like phenotype. Curr. Biol. **14:**2264-70.

42. **Wang, X., and P. Baumann.** 2008. Chromosome fusions following telomere loss are mediated by single-strand annealing. Mol. Cell **31:**463-73.

43. **Win, T. Z., H. W. Mankouri, I. D. Hickson, and S. W. Wang.** 2005. A role for the

fission yeast Rqh1 helicase in chromosome segregation. J. Cell. Sci. **118:**5777-84.

44. **Wu, L., A. S. Multani, H. He, W. Cosme-Blanco, Y. Deng, J. M. Deng, O. Bachilo, S. Pathak, H. Tahara, S. M. Bailey, Y. Deng, R. R. Behringer, and S. Chang.** 2006. Pot1 deficiency initiates DNA damage checkpoint activation and aberrant homologous recombination at telomeres. Cell **126:**49-62.

45. **Xhemalce, B., J. S. Seeler, G. Thon, A. Dejean, and B. Arcangioli.** 2004. Role of the fission yeast SUMO E3 ligase Pli1p in centromere and telomere maintenance. EMBO J. **23:**3844-53.

46. **Yang, Q., Y. L. Zheng, and C. C. Harris.** 2005. POT1 and TRF2 cooperate to maintain telomeric integrity. Mol. Cell. Biol. **25:**1070-80.

47. **Zhu, Z., W. H. Chung, E. Y. Shim, S. E. Lee, and G. Ira.** 2008. Sgs1 helicase and two nucleases Dna2 and Exo1 resect DNA double-strand break ends. Cell **134:**981-94.

FIGURE LEGENDS

Figure 1. ***pot1Δ rqh1-hd*** **double mutant is viable, but is sensitive to TBZ.** (**A**) Spotting assay of 10-fold serial dilutions of cells. The plasmid is retained on EMM plus adenine and leucine, and selected against on YEA plus FUDR at 30°C. (**B** and **C**) The sensitivities to temperature (B) and TBZ (C) of wild-type, *rqh1-hd, pot1Δ*, and 2 independent *pot1Δ rqh1-hd* cells were determined using a spot test. The 10-fold dilutions of log-phase cells were spotted onto a YEA plate at the indicated temperature or a YEA plate containing 12.5 μg/mL TBZ at 30°C.

Figure 2. ***pot1Δ rqh1-hd*** **double mutant can maintain telomeres that are dependent on HR activity.** (**A**) Restriction enzyme sites around the telomeric (Telo) and telomere-associated sequence (TAS1) of 1 chromosome arm cloned in the plasmid pNSU70 (36). **(B)** The telomere length of the wild-type, *rqh1-hd*, and *pot1Δ rqh1-hd* cells was analyzed using Southern hybridization at 25°C. Genomic DNA was digested with *EcoR*I, separated by 1.5% agarose gel electrophoresis, and hybridized to a 450-bp synthetic telomere fragment as probe, or a 700-bp DNA fragment containing the TAS1 sequence. To assess the total amount of DNA, the gel was stained with ethidium bromide (EtBr) before blotting onto the membrane. (**C**) BAL31 nuclease treatment of genomic DNA from wild-type and *pot1Δ rqh1-hd* cells. Samples were digested with 4 units of BAL31 nuclease (NEB) for 5 or 10 hours. After the BAL31 treatment, genomic DNA was analyzed as shown in (B). (**D**) Schematic diagram of telomeric structure in wild-type and *pot1Δ rqh1-hd* cells. Telomeric sequences are indicated as wiggle line. TAS1 containing subtelomeric elements are indicated as a box. Vertical arrows indicate the position of *EcoR*I digestion. The canonical positions of

TSA1 sequence are indicated by line below the box. (**E**) The telomere length of the *pot1Δ rqh1-hd* cells and *pot1Δ rqh1-hd rad51Δ* cells was analyzed using Southern hybridization at 25°C. Genomic DNA was digested with *EcoR*I and hybridized to a 1-kbp DNA fragment containing telomere plus TAS1 sequences.

Figure 3. ***pot1Δ rqh1-hd*** **double mutant chromosomes are not circularized, but the chromosome ends are entangled.** (**A**) *Not*I restriction enzyme map of *S. pombe* chromosomes. Chromosomes I, II, and III (Ch. I, Ch. II, and Ch. III) are shown. (**B**) *Not*I-digested *S. pombe* chromosomal DNA from the *rqh1-hd* cells and 2 independent *pot1Δ rqh1-hd* cells that were incubated at 25°C was analyzed using PFGE. Probes specific for the *Not*I fragments (C, I, L, and M) and Nbs1 were used (31). The non-specific bands detected in *rqh1-hd* and *pot1Δ rqh1-hd* cells are shown by asterisks. To assess the total amount of DNA, the gel was stained with ethidium bromide (EtBr) before blotting onto the membrane. (**C**) *Not*I-digested *S. pombe* chromosomal DNA of wild-type cells, *pot1Δ rqh1-hd rad51Δ* cells, and *pot1Δ* cells was analyzed using PFGE. The probes specific for the *Not*I fragments (C, I, L, and M) were used.

Figure 4. ***pot1Δ rqh1-hd*** **double mutant has RPA foci, and the Taz1 (telomere) foci and the Rad22 (Recombination) foci colocalize with the Ssb2 (RPA) foci.** (**A**) Visualization of RPA foci in asynchronous living cells. Vegetatively growing wild-type cells, *rqh1-hd* cells, and *pot1Δ rqh1-hd* cells, in which Rad11 is endogenously tagged with GFP, were observed at 30°C. Bar = 5 μm. (**B**) RPA foci in **A** are categorized as no foci, 1 dot, 2 dots, 3 dots, and a Bright cluster. The y-axis indicates the percentage of cells. The total cell number examined

(N) is shown at the top. (**C**) Merged images of fluorescence micrographs showing Ssb2-Cerulean (Red) and Taz1-YFP (Green) at 30°C. The middle subunit of RPA (Ssb2) and Taz1 were endogenously tagged with Cerulean (a CFP variant) and YFP in the *pot1Δ rqh1-hd* double mutant, respectively. *pot1Δ rqh1-hd* expressing Pot1 from a plasmid, which behaves like the *rqh1-hd* single mutant, was used as a control. The arrow and arrowhead indicate colocalization and adjacent localization, respectively. (**D**) The percentages of the Taz1 foci that colocalized with (colocalization) or were adjacent to the RPA foci (side by side) are presented. The total cell number examined (N) is shown at the top. (**E**) Merged images of fluorescence micrographs showing Ssb2-Cerulean (Red) and Rad22-YFP (Green) at 30°C. The middle subunit of RPA (Ssb2) and Rad22 were endogenously tagged with Cerulean (a CFP variant) and YFP in the *pot1Δ rqh1-hd* double mutant, respectively. (**F**) The percentage of the Rad22 foci that colocalized with the RPA foci is presented. The total cell number examined (N) is shown at the top.

Figure 5. **The *pot1Δ rqh1-hd* double mutant and *rqh1-hd* single mutant released from S phase arrest have RPA foci during the M phase.** (**A**) Visualization of RPA foci during the M phase in asynchronous living cells. Rad11-GFP-expressing living *rqh1-hd* cells and *pot1Δ rqh1-hd* cells cells were observed in a series of time lapse images taken at 1 min intervals at 30°C. Bar = 5 μm. The time 0 represents the time just before entering anaphase. (**B**) Percentages of cells in which the RPA foci appeared on the chromosome bridges in **A** are shown. The data from the analysis of the Rad11-mRFP-expressing living *pot1Δ rqh1-hd rad51Δ* was also added. The total number of M phase cells that were observed in this experiment (N) is shown at the top. (**C**) Visualization of RPA foci during the M phase in

rqh1-hd cells released from S phase arrest. Rad11-GFP-expressing living *rqh1-hd* cells released from S phase arrest were observed at 30°C. We added 10 mM HU to an asynchronous culture of Rad11-GFP-expressing *rqh1-hd* cells in YEA medium. After 4 h in HU, the cells were washed and transferred to YEA medium without HU and cultured for a further 2 h. The resulting cells were observed. 2 different *rqh1-hd* cells are shown. Bar = 5 μm. (**D**) Percentages of *rqh1-hd* cells in which the RPA foci appeared on chromosome bridges in **C** are shown. The total number of M phase cells that were observed in this experiment (N) is shown at the top. (**E**) RPA foci in the *pot1Δ rqh1-hd* double mutant do not colocalize with Gar2 (rDNA). Merged images of fluorescence micrographs showing Rad11-mRFP (Red) and Gar2-GFP (Green) in the 2 different *pot1Δ rqh1-hd* double-mutant cells during the M phase at 30°C.

Figure 6. ***pot1Δ rqh1-hd*** **double mutant has a defect in chromosome segregation.** (**A**) Percentage of defects in chromosome segregation in asynchronous living cells. The indicated concentrations of TBZ were added to an asynchronous culture of Rad11-GFP-expressing *rqh1-hd* cells and *pot1Δ rqh1-hd* cells in YEA medium for 4 h. The resulting cells were observed at 30°C. As RPA localizes to the entire nucleus, chromosome segregation defects were monitored by the localization of RPA. The total number of asynchronous living cells that were observed in this experiment (N) is shown at the top. The y-axis indicates the percentage of cells that display the cut or non-disjunction phenotype. (**B**) An example of the cut phenotype (in the presence of 17.5 μg/mL TBZ, left panel, and in the presence of 50 μg/mL TBZ, middle panel) and non-disjunction (in the presence of 50 μg/mL TBZ, right panel) in *pot1Δ rqh1-hd* cells are shown. (**C**) Model for chromosome segregation defects in *pot1Δ*

rqh1-hd double mutant. One pair of sister chromatids in the *pot1Δ rqh1-hd* double mutant, in which the telomeres are entangled during the M phase, is shown. The kinetochore/centromere is shown by a small circle. The mitotic spindle between the kinetochore/centromere is shown by a thick line. The mitotic spindle is destabilized in the presence of TBZ (shown by a thin line).

Figure 7. **POT1 and WRN deficiencies render human cultured cells sensitive to vinblastine.** (**A and B**) (**A**) Establishment of the cell lines. WRN-deficient W-V cells were infected with the retrovirus for FLAG-tagged WRN (W-V/WRN). W-V/pLPC is a mock infectant used as the control. The TNE lysates were prepared and subjected to immunoprecipitation (IP), followed by western blot analysis (WB). HeLa I.2.11 cells were used as a control for the detection of endogenous WRN. IgG, normal immunoglobulin G. *Values* indicate the protein size markers. (**B**) POT1 depletion using siRNA. The cells were transfected with the indicated siRNA. After a 48-h incubation, the TNE lysates were subjected to IP, followed by western blot analysis. IgH, immunoglobulin heavy chain. (**C**) Effects of POT1 and WRN deficiencies on the sensitivity to vinblastine, an inhibitor of microtubule polymerization. The cells were transfected with the indicated siRNA for 24 h, and then incubated with various concentrations of vinblastine for 48 h. Cell number (%) refers to the cell counts normalized to those in the absence of vinblastine. *Error bars* indicate the standard deviation of 3 to 4 independent experiments, each performed in triplicate. (**D**) Reconstitution of WRN counteracts the POT1 knockdown-induced sensitization to vinblastine in W-V cells. Sensitization to vinblastine (ratio of IC50 values of control siRNA-treated cells to those of POT1 knockdown cells) was determined from **(C)**. *Error bars* indicate the standard deviation

of 3 to 4 independent experiments. *Asterisk* indicates a statistically significant difference ($p < 0.05$).

Table.1

Strain	Genotype	**source**
JY741	*h⁻ leu1-32 ura4-D18 ade6-M216*	M. Yamamoto
PP74-No.4	*h⁺ leu1-32 ura4-D18 ade6-M210 pot1::kanMX*	P. Baumann
MGF809	*h⁻ ura4-D18 rad11-GFP::kanMX*	M. Ferreira
YK002	*h⁺ leu1-32 ura4-D18 ade6-M210 rqh1-K547A*	This study
GT000	*h⁺ leu1-32 ura4-D18 ade6-M210 rqh1-K547A pot1::kanMX pPC27-pot1⁺-HA*	This study
GT001	*h⁺ leu1-32 ura4-D18 ade6-M210 rqh1-K547A pot1::kanMX rad51::LEU2*	This study
GT002	*h⁺ leu1-32 ura4-D18 ade6-M210 rqh1-K547A pot1::kanMX*	This study
TH001	*h⁺ leu1-32 ura4-D18 ade6-M216 rqh1:: hphMX pot1::kanMX pPC27-pot1⁺-HA*	This study
KTA002	*h⁻ ura4-D18 pot1::kanMX6 rqh1-K547A rad11-GFP::kanMX6*	This study
KTA003	*h⁺ ura4-D18 ade6-M216 rqh1-K547A rad11-GFP::kanMX6*	This study
KTA006	*h⁺ leu1-32 ura4-D18 ade6-M210 pot1::kanMX6 rqh1-K547A pPC27-pot1⁺-HA taz1-YFP::kanMX6 ssb2-Cerulean::kanMX6*	This study
KTA007	*h⁺ leu1-32 ura4-D18 ade6-M210 pot1::kanMX6 rqh1-K547A taz1-YFP::kanMX6 ssb2-Cerulean::kanMX6*	This study
KTA010	*h⁻ leu1-32 ura4-D18 ade6-M216 pot1::kanMX6 rqh1-K547A rad11-mRFP::natMX6 gar2-GFP::kanMX6*	This study
KTA018	*h⁻ leu1-32 ura4-D18 ade6-M210 pot1::kanMX6 rqh1-K547A rad22-YFP::kanMX6*	This study
KTA020	*h⁻ leu1-32 ura4-D18 ade6-M210 pot1::kanMX6 rqh1-K547A rad22-YFP::kanMX6 ssb2-Cerulean::kanMX6*	This study
KTA022	*h⁺ leu1-32 ura4-D18 ade6-M210 rqh1-K547A pot1::kanMX rad51::LEU2 rad11-mRFP::natMX6*	This study

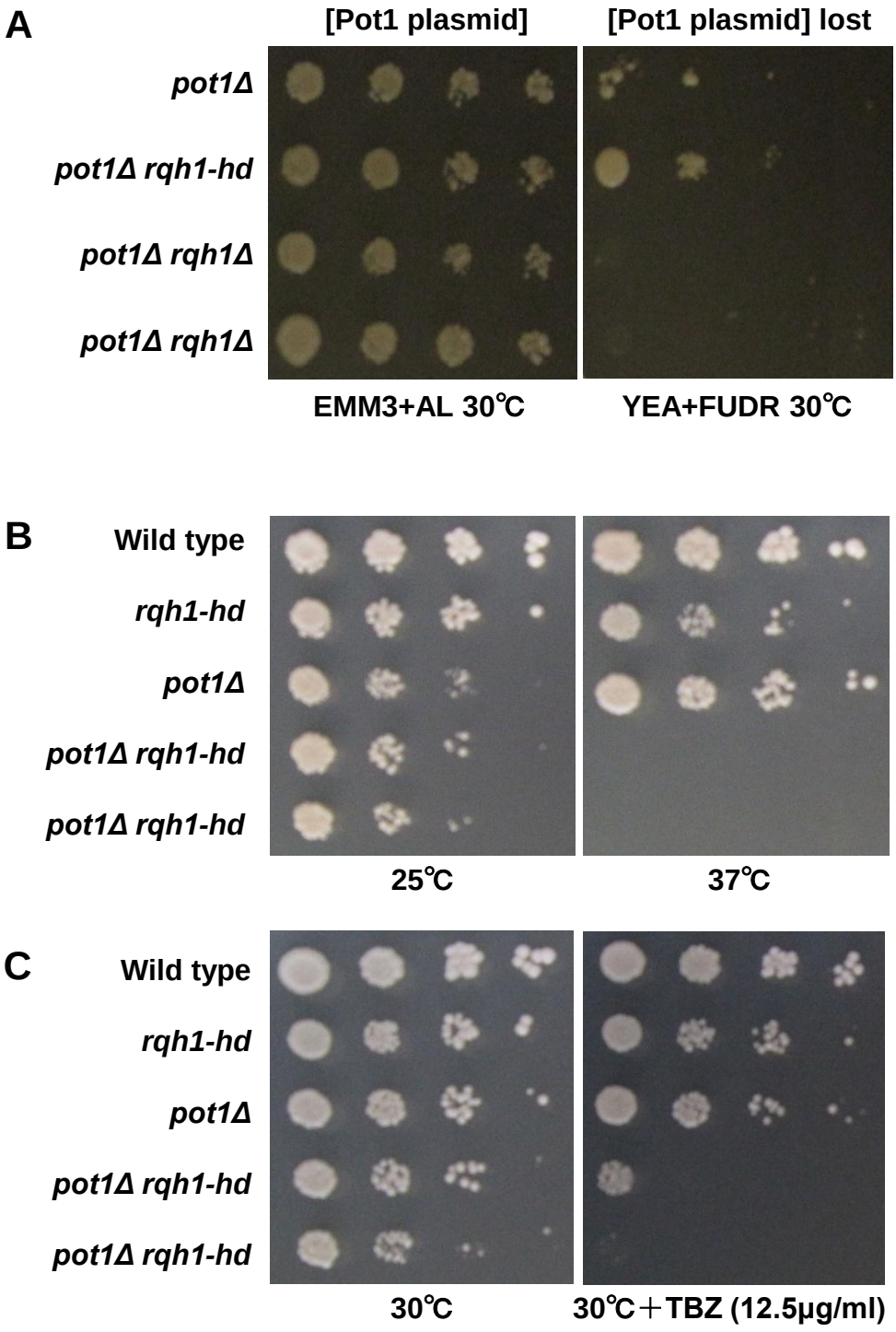
A
[Pot1 plasmid]
[Pot1 plasmid] lost
pot1Δ
pot1Δ rqh1-hd
pot1Δ rqh1Δ
pot1Δ rqh1Δ
EMM3+AL 30℃
YEA+FUDR 30℃
B
Wild type
rqh1-hd
pot1Δ
pot1Δ rqh1-hd
pot1Δ rqh1-hd
25℃
37℃
C
Wild type
rqh1-hd
pot1Δ
pot1Δ rqh1-hd
pot1Δ rqh1-hd
30℃
30℃＋TBZ (12.5μg/ml)

Figure 1.

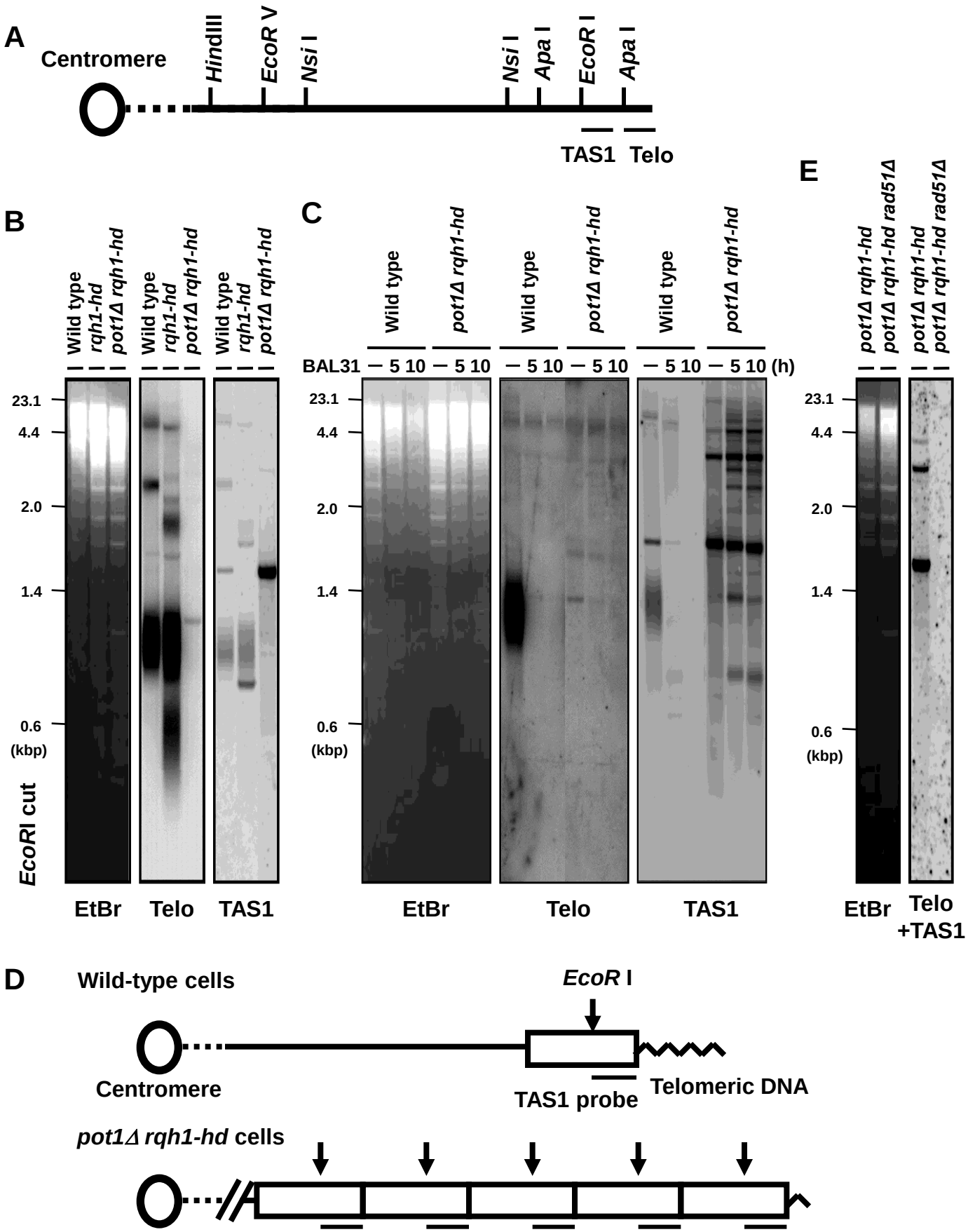
A
Centromere
HindIII
EcoR V
Nsi I
Nsi I
Apa I
EcoR I
Apa I
TAS1
Telo
B
Wild type
rqh1-hd
pot1Δ rqh1-hd
23.1
4.4
2.0
1.4
0.6
(kbp)
EcoRI cut
EtBr
Telo
TAS1
C
Wild type
pot1Δ rqh1-hd
BAL31 – 5 10 (h)
EtBr
Telo
TAS1
E
pot1Δ rqh1-hd
pot1Δ rqh1-hd rad51Δ
EtBr
Telo +TAS1
D
Wild-type cells
EcoR I
Centromere
TAS1 probe
Telomeric DNA
pot1Δ rqh1-hd cells

Figure 2.

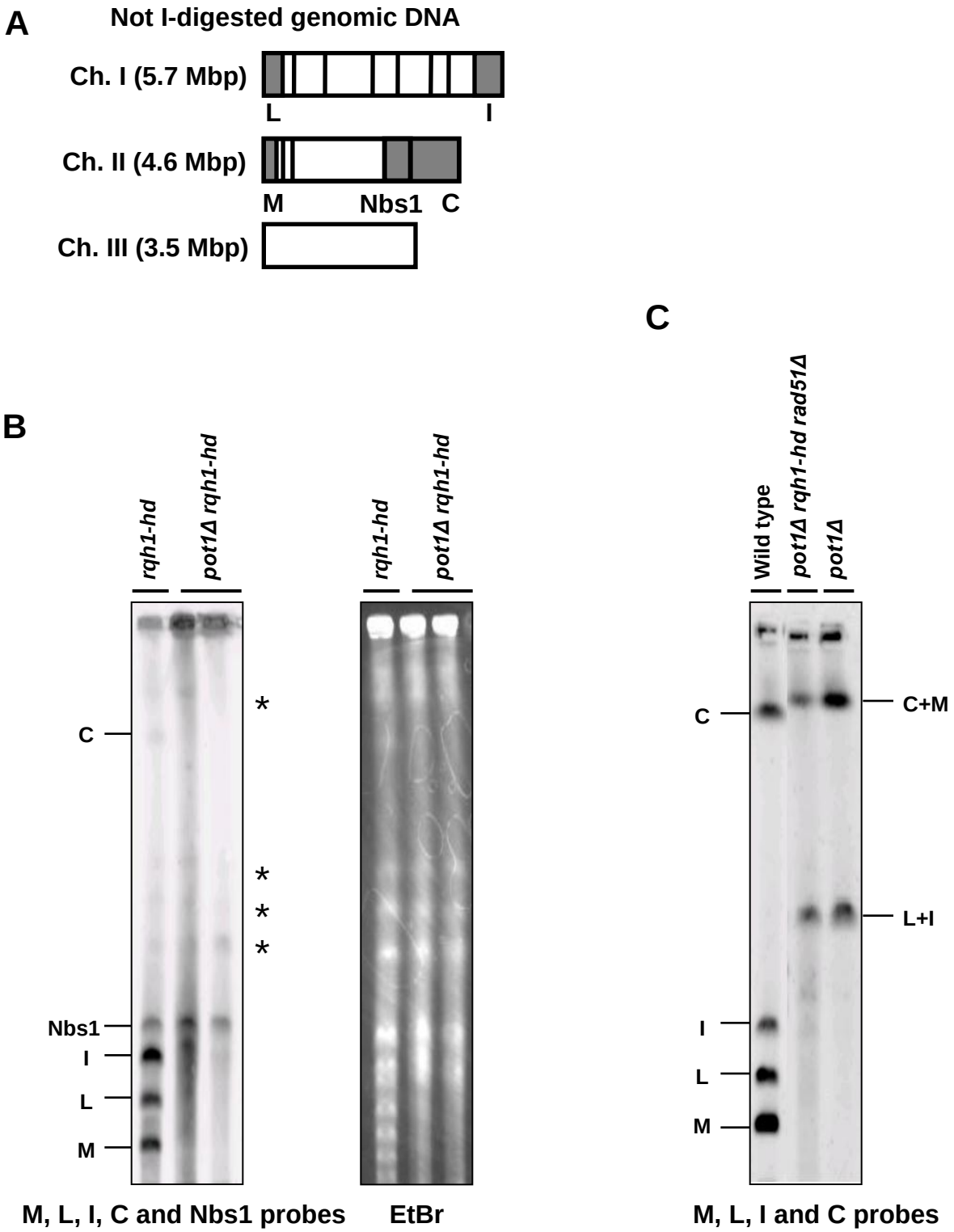
A
Not I-digested genomic DNA
Ch. I (5.7 Mbp)
L
I
Ch. II (4.6 Mbp)
M
Nbs1
C
Ch. III (3.5 Mbp)
B
rqh1-hd
pot1Δ rqh1-hd
rqh1-hd
pot1Δ rqh1-hd
C
*
*
*
*
Nbs1
I
L
M
M, L, I, C and Nbs1 probes
EtBr
C
Wild type
pot1Δ rqh1-hd rad51Δ
pot1Δ
C+M
L+I
C
I
L
M
M, L, I and C probes

Figure 3.

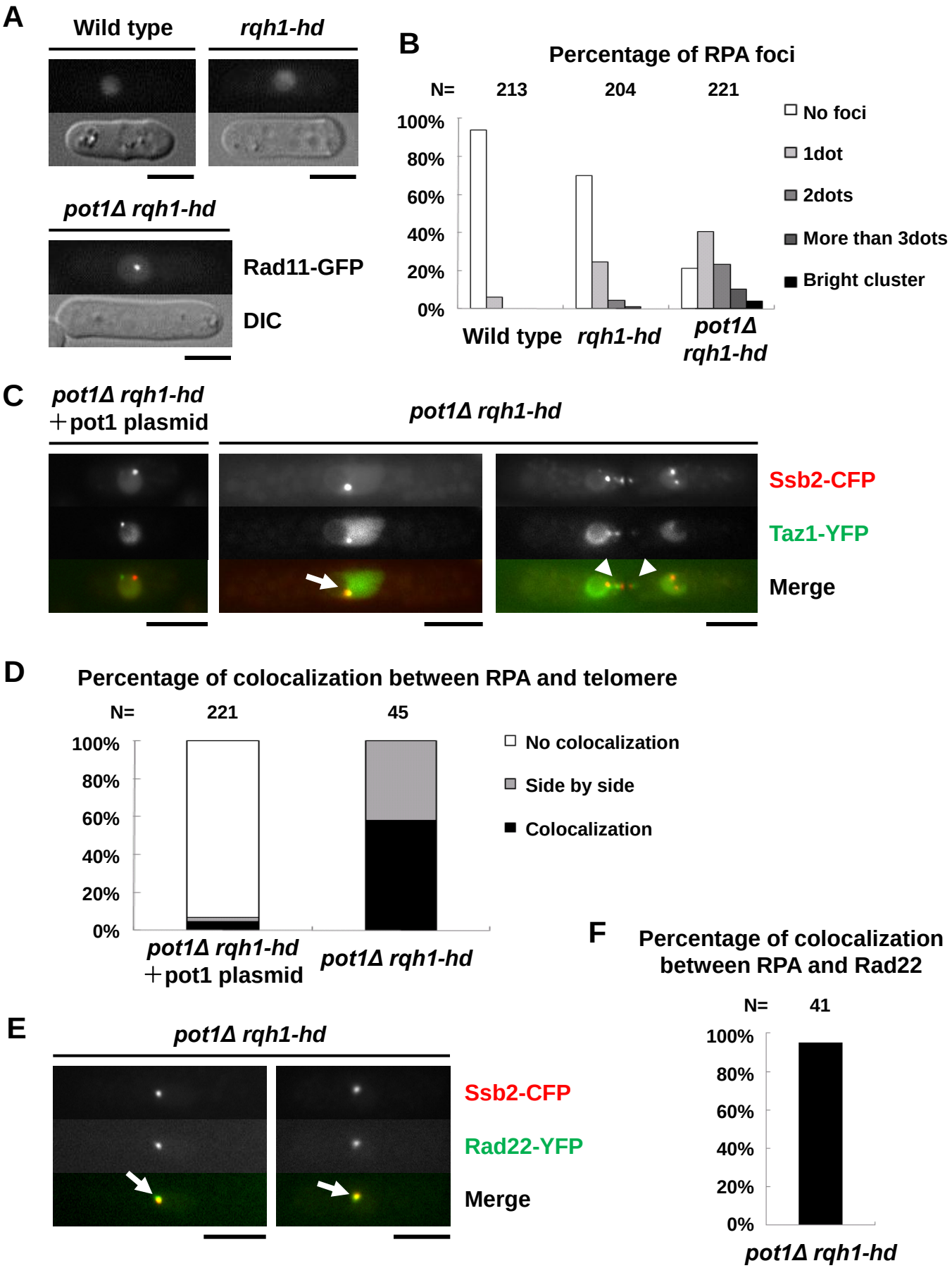
A
Wild type
rqh1-hd
pot1Δ rqh1-hd
Rad11-GFP
DIC
B
Percentage of RPA foci
N=
213
204
221
100%
80%
60%
40%
20%
0%
No foci
1dot
2dots
More than 3dots
Bright cluster
Wild type
rqh1-hd
pot1Δ rqh1-hd
C
pot1Δ rqh1-hd +pot1 plasmid
pot1Δ rqh1-hd
Ssb2-CFP
Taz1-YFP
Merge
D
Percentage of colocalization between RPA and telomere
N=
221
45
100%
80%
60%
40%
20%
0%
No colocalization
Side by side
Colocalization
pot1Δ rqh1-hd +pot1 plasmid
pot1Δ rqh1-hd
E
pot1Δ rqh1-hd
Ssb2-CFP
Rad22-YFP
Merge
F
Percentage of colocalization between RPA and Rad22
N=
41
100%
80%
60%
40%
20%
0%
pot1Δ rqh1-hd

Figure 4.

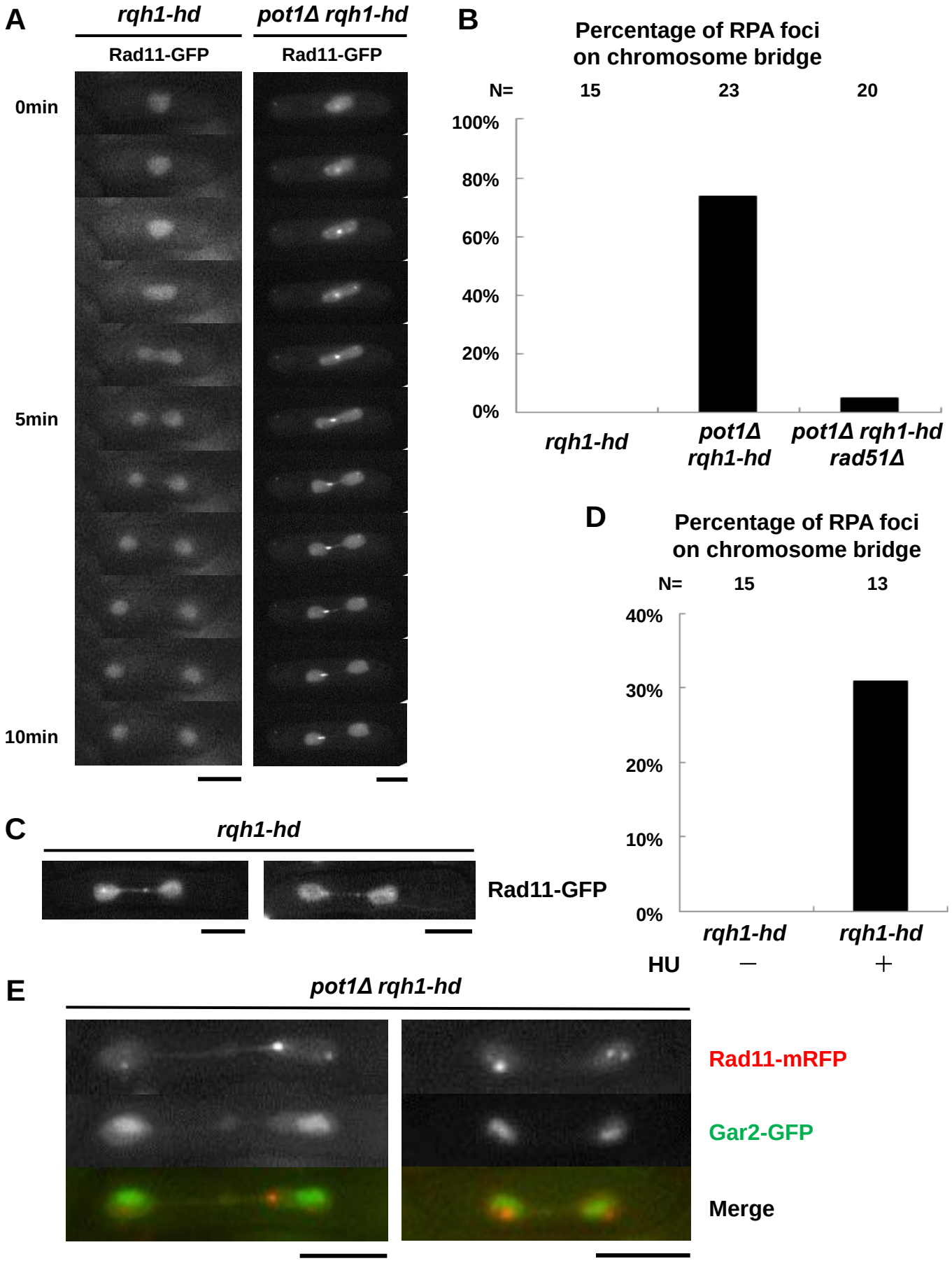
A
rqh1-hd
pot1Δ rqh1-hd
Rad11-GFP
Rad11-GFP
0min
5min
10min
B
Percentage of RPA foci
on chromosome bridge
N=
15
23
20
100%
80%
60%
40%
20%
0%
rqh1-hd
pot1Δ
rqh1-hd
pot1Δ rqh1-hd
rad51Δ
C
rqh1-hd
Rad11-GFP
D
Percentage of RPA foci
on chromosome bridge
N=
15
13
40%
30%
20%
10%
0%
rqh1-hd
rqh1-hd
HU
–
+
E
pot1Δ rqh1-hd
Rad11-mRFP
Gar2-GFP
Merge

Figure 5.

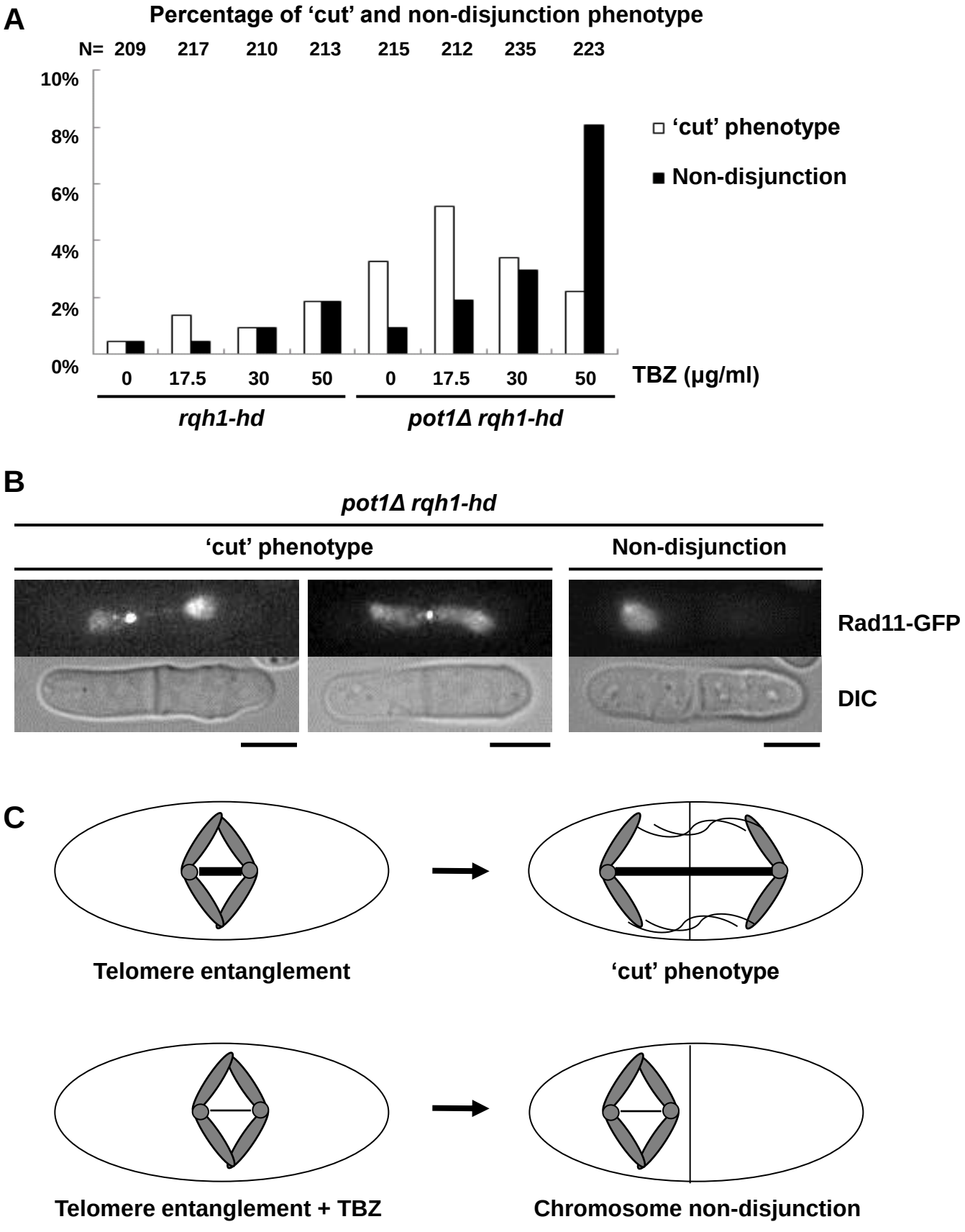
A
Percentage of 'cut' and non-disjunction phenotype
N= 209 217 210 213 215 212 235 223
10%
8%
6%
4%
2%
0%
'cut' phenotype
Non-disjunction
0 17.5 30 50 0 17.5 30 50
TBZ (μg/ml)
rqh1-hd
pot1Δ rqh1-hd
B
pot1Δ rqh1-hd
'cut' phenotype
Non-disjunction
Rad11-GFP
DIC
C
Telomere entanglement
'cut' phenotype
Telomere entanglement + TBZ
Chromosome non-disjunction

Figure 6.

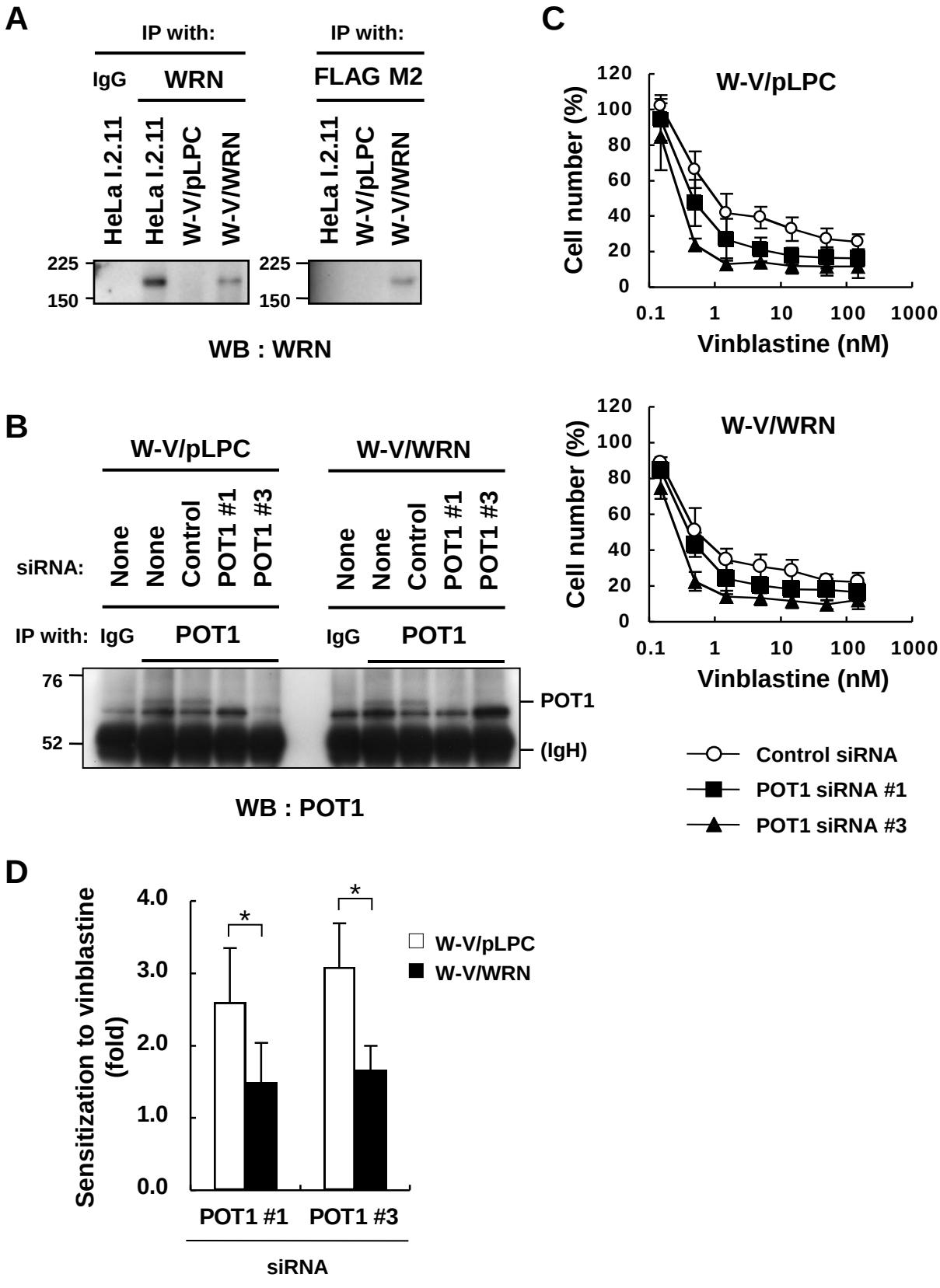
A
IP with:
IgG
WRN
IP with:
FLAG M2
HeLa I.2.11
HeLa I.2.11
W-V/pLPC
W-V/WRN
HeLa I.2.11
W-V/pLPC
W-V/WRN
225
150
225
150
WB : WRN
B
W-V/pLPC
W-V/WRN
siRNA:
None
None
Control
POT1 #1
POT1 #3
None
None
Control
POT1 #1
POT1 #3
IP with:
IgG
POT1
IgG
POT1
76
52
POT1
(IgH)
WB : POT1
C
W-V/pLPC
Cell number (%)
120
100
80
60
40
20
0
0.1
1
10
100
1000
Vinblastine (nM)
W-V/WRN
Cell number (%)
120
100
80
60
40
20
0
0.1
1
10
100
1000
Vinblastine (nM)
Control siRNA
POT1 siRNA #1
POT1 siRNA #3
D
Sensitization to vinblastine (fold)
4.0
3.0
2.0
1.0
0.0
*
*
W-V/pLPC
W-V/WRN
POT1 #1
POT1 #3
siRNA

Figure 7.